PHYSICAL REVIEW D VOLUME 15, NUMBER 7 1 APRIL 1977

Baryon-exchange Deck-model contributions to nucleon diffraction dissociation*

Roger T. Cutler and Edmond L. Berger
High Energy Physics Division, Argonne National Laboratory, Argonne, Illinois 60439
(Received 14 January 1977)

In a Drell-Deck-model description of high-energy nucleon diffraction dissociation, $aN \to a(N\pi)$, we study the contributions which the baryon-exchange and direct-baryon-pole Deck graphs make to the production and decay distributions of the low-mass $N\pi$ system. We treat spin effects explicitly. Because the two baryon amplitudes cancel each other to a remarkable degree, their sum has only a small effect ($\sim 20\%$) on the overall cross section, which is dominated by the pion-exchange Deck amplitude. Nevertheless, the baryon terms have an important influence on the decay angular distributions of the $N\pi$ system, particularly in that region of phase space in which the pion-exchange term is suppressed. They also provide a pronounced increase in the slope of the production-momentum-transfer (t) distribution near the $N\pi$ threshold. Both of these results improve the agreement of the unabsorbed Deck model with recent data on $NN \to N(N\pi)$ from Fermilab and the CERN ISR. Discrepancies remain in the description of certain correlations between structure in the t distribution and selections on the decay angles. We speculate that this failure suggests the presence of a second non-Deck, perhaps resonant, component in the data and the necessity for a coupled analysis in which final-state interactions are included.

I. INTRODUCTION

Our perception of diffraction in hadronic processes has been enriched considerably as a result of very-high-energy elastic and inelastic scattering experiments at Serpukhov, Fermilab, and the CERN Intersecting Storage Rings (ISR). In particular, studies of the exclusive nucleon (N) dissociation process $NN \to N(N\pi)$ have provided evidence for the diffractive excitation of a broad, low-mass $N\pi$ continuum with fine structure in mass of a resonance nature.[1,2,3] While both resonant and continuum components are visible in lower-energy data, the high-energy experiments at the ISR and at Fermilab have shown that both survive asymptotically (i.e., are "diffractive"). As a result of the precision of these investigations, new remarkable properties of the production and decay distributions of the $N\pi$ system were also discovered.[1,2] In this article we discuss a dynamical interpretation of the diffractive continuum in terms of the Drell-Deck model. We also consider briefly the addition of resonance effects.

The Drell-Deck model[4,5,6] has been used in attempts to describe the nonresonant diffractive continuum in $Np \to (N\pi)p$ and in other similar processes.[6] In most calculations, attention is restricted to a computation of the unabsorbed π-exchange Deck graph illustrated in Fig. 1(a). This term alone provides an adequate average description of many aspects of the data, including a high degree of correlation between the production and decay systematics. It was argued,[6,7] however, that specific features of the data, such as structure in decay angular distributions of the type since observed[1-3] and crossover properties of t distributions, may serve as qualitative evidence that other exchange terms are important. In a study[8] of $\pi^{\pm}p \to \pi^{\pm}(\pi^{-}\Delta^{++})$, such evidence supports the need for a baryon-exchange term in addition to the π-exchange contribution. The baryon-exchange Deck graphs are illustrated in Figs. 1(b) and 1(c) for the diffractive reaction $ap \to a(N\pi)$, where a is any hadron. These graphs have been treated previously in various approximations.[3,9,10] It is our intention here to demonstrate the extent to which inclusion of the baryon terms improves the quantitative description of the high-energy data, emphasizing the decay angular distributions.

Baryon exchange is notoriously difficult to parametrize even in high-energy elastic processes,[11] and our expectations for success in an inelastic process must be correspondingly modest. We will examine in detail three theoretical aspects of N-exchange Deck models including an explicit treatment of spin: (1) We show how N-exchange [Fig. 1(b)] and direct-production [Fig. 1(c)] amplitudes tend to cancel, $B + D \approx 0$, and we explore how this cancellation affects various observables. (2) We consider two possible helicity structures (s-channel and t-channel helicity conservation) for the $Na \to Na$ diffractive amplitude which is a component of the Deck model, and we show that neither is excluded by the inelastic data. (3) We show how form factors in the baryon propagator can be chosen judiciously to alter the spin-parity content of the *virtual* nucleon, and we observe that certain versions of the model are insensitive to the relative amounts of $J^P = \frac{1}{2}^+$ and $\frac{1}{2}^-$ (parity doublet) components in the propagator. We employ high-energy

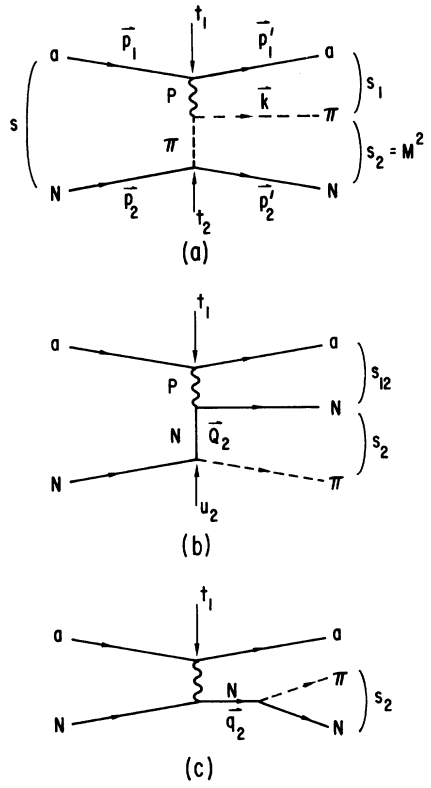

FIG. 1. The three Deck-model diagrams for $aN \to a(\pi N)$. Kinematic variables are indicated in (a) and (b).

assumptions throughout; for example, we do not distinguish between the diffractive amplitudes for $\pi^+ a \to \pi^+ a$ and $\pi^- a \to \pi^- a$. In this sense we calculate a Deck model for the process $aN \to a(\pi N)$, where only isospin zero is exchanged at the $a\bar{a}$ vertex. However, there are identical-particle counting factors and isospin coupling coefficients which differ for different realizations of this reaction. Unless otherwise specified, all cross sections we present are for the process $pn \to p(\pi^- p)$ at 100 GeV/c. Other cross sections can be obtained from our results by multiplying by suitable factors: a counting factor of 2 if there are identical particles in the initial state [e.g., $pp \to p(\pi^+ n)$], an isospin factor of $\frac{1}{2}$ if the pion is neutral [e.g., $np \to n(\pi^0 p)$].

In Sec. II we will present our simple version of the π-exchange Deck-model amplitude, Π. The baryon-exchange amplitude, B, and a direct-production amplitude, D, are presented in Sec. III, and the s-channel (model s) and t-channel (model t) helicity-conserving diffractive amplitudes are introduced. In Sec. IV we discuss technical aspects of the computation, notably the evaluation of the spin sums. The remarkable cancellation of B and D, $|B+D|^2 \cong 0$, is explored in Sec. V. In Sec. VI we present some comparisons with data. We show that the baryon terms improve substantially the agreement of the model with data on the decay angular distributions of the $N\pi$ system in that region of phase space in which the Π amplitude is suppressed. In model s the baryon terms also provide a pronounced increase in the logarithmic slope of the production-momentum-transfer t_1 distribution $d\sigma/dt_1 dM_{N\pi}$ for $M_{N\pi}$ near threshold, in fair agreement with data. Discrepancies which remain with absolute normalization and in the description of certain correlations between structure in $d\sigma/dt_1$ and selections on the $N\pi$ decay angles are also discussed. Conclusions and our outlook are summarized in Sec. VII. In the Appendix, we discuss how form factors can be chosen in such a way as to modify the spin parity of the virtual baryon. For the remainder of the introduction, we provide a summary of the experimental situation and a qualitative description of our approach.

The CERN-Hamburg-Orsay-Vienna group[2] has investigated the process $pp \to p(n\pi^+)$ at the ISR Split-Field Magnet Facility, and a Rochester-Fermilab-SLAC-Northwestern group[1] has studied $np \to (p\pi^-)p$ at Fermilab. In addition to the broad, low-mass $N\pi$ continuum with resonant fine structure mentioned above, both groups demonstrate that the production-momentum-transfer distribution $d\sigma/dt_1$ for $NN \to N(N\pi)$ has sharp structure near $|t_1| = 0.2$ GeV^2 for small values of $M_{N\pi}$ (<1.5 GeV). The interpretation of this structure is of substantial interest from several points of view. If one *assumes* that the structure corresponds to a zero near $|t_1| = 0.2$ GeV^2 in one dominant non-spin-flip exchange *amplitude*, then the structure is direct evidence for the "peripheral" character of inelastic diffraction. This conclusion is remarkable in that *elastic* diffraction is by contrast a "central" process in impact-parameter space, an inference drawn from the nearly exponential behavior of the elastic differential cross section out to $|t_1| \simeq 1$ GeV^2. It is essential to verify these significant conclusions by extracting from data the behavior in impact parameter of the different spin amplitudes using, for example, the Argonne polarized-beam facility.

The apparently peripheral character of inelastic diffraction is suggestive of a constituent interpretation of the nucleon. In the Deck model, the nucleon "constituents" in $ap \to a(N\pi)$ are the (off-shell) final N and π themselves. From this perspective, a reproduction of the diffractive structure near $|t_1| = 0.2$ GeV^2 may be sought in terms of rescattering (absorptive) corrections to the Deck amplitudes.[12] While the absorbed-Deck-model approach provides a qualitative interpretation of some aspects of the data,[12] the structure generated is generally at larger $|t_1|$ (~0.3 GeV^2) and/or is

less pronounced than in the data.

Within the context of the Deck model, absorptive corrections may well not be the proper interpretation of the structure near $|t_1| = 0.2$ GeV^2. In this regard, one additional systematic feature of the data deserves emphasis here and will be treated further in the text. For fixed excitation mass, M, the diffractive structure in $|t_1|$ is shown to be most pronounced for values of the t-channel polar angle $\theta_t \simeq \pi/2$ in the $N\pi$ rest frame. For forward ($\theta_t \simeq 0$) and backward ($\theta_t \simeq \pi$) decay angles, structure is notably absent, and the unabsorbed Deck model is entirely adequate (c.f., Sec. VI). In a theoretical context, this may suggest that, instead of absorption, there is an additional non-Deck (e.g., resonant) contribution which is particularly significant for $\theta_t \simeq \pi/2$, where the Deck terms are relatively less important. If these hypothetical "resonance" waves are produced peripherally, the structure in $|t_1|$ follows. It may also be true that both the Deck and resonant components are featureless in $|t_1|$ and that the observed structure arises from interference of the two components. One can construct models of either variety. If the structure in $|t_1|$ is a Deck–non-Deck interference, the idea that inelastic diffraction is peripheral might be seriously undermined. In an attempt to separate the components and to determine their production characteristics, a partial-wave analysis of the data is essential. Obviously, data obtained from the dissociation of a polarized beam or target are required.

II. PION EXCHANGE

We take an entirely conventional, albeit somewhat unsophisticated, approach to the π-exchange graph shown in Fig. 1(a) for the reaction $aN \to a(\pi N)$, where a is a hadron. The ingredients of the model are as follows: (1) a Feynman propagator for the exchanged pion, (2) a $\pi\pi N$ vertex factor $ig\gamma_5$, where g is the πN coupling constant, $g_{pp\pi^0}{}^2 = 4\pi(14.5)$, (3) a form factor, $F_\pi(t_2)$, which we take to be an exponential, (4) an invariant amplitude, $\mathfrak{M}_{\pi a}$, for the diffractive process $\pi a \to \pi a$, with the initial-state pion off the mass shell.

The π-exchange invariant amplitude for $an \to a(p\pi^-)$ is then

$$\mathfrak{M}_\pi = \bar{u}(p_2') \frac{i\sqrt{2}\, g\gamma_5 F_\pi(t_2)}{t_2 - \mu^2} \mathfrak{M}_{\pi a}(s_1) u(p_2), \tag{2.1}$$

$$F_\pi(t_2) = \exp(-\tfrac{1}{2} b_\pi |t_2 - \mu^2|), \tag{2.2}$$

where μ is the pion mass. An additional isospin-related factor of $\sqrt{2}$ appears on the right-hand side of Eq. (2.1) for the dissociations $p \to n\pi^+$ or $n \to p\pi^-$. In general, the amplitude $\mathfrak{M}_{\pi a}$ depends not only on s_1 and t_1, but also on the spin projections of particle a and the mass, t_2, of the virtual pion. However, in the usual spirit of the Deck model, we make simplifying assumptions about this amplitude. In the diffractive limit of large s_1 and small t_1, the scattering angle of the a in the πN rest frame is small (of order t_1/s_1), and hence the detailed spin structure of the $a\bar{a}$ vertex contributes only nonasymptotic correction terms to the amplitude. We may thus use a spin-averaged approximation for $\mathfrak{M}_{\pi a}$ in the large-s limit. Considering only Pomeron exchange, we write

$$\mathfrak{M}_{\pi a}(s_1) = i s_1 \sigma_{\pi a} \exp(\tfrac{1}{2} b_{\pi a} t_1), \tag{2.3}$$

and, assuming the off-mass-shell corrections to be small, we take $\sigma_{\pi a}$ and $b_{\pi a}$ to be the total cross section and elastic slope of the on-shell πa interaction. The spin sums are easily performed. We obtain

$$|\Pi|^2 \equiv \tfrac{1}{2} \operatorname{Tr}(\bar{\mathfrak{M}}_\pi \mathfrak{M}_\pi) = 2g^2 \sigma_{\pi a}{}^2 \frac{-t_2 F_\pi{}^2(t_2)}{(t_2 - \mu^2)^2} s_1{}^2 \exp(b_{\pi a} t_1). \tag{2.4}$$

This approach to the π-exchange Deck model is virtually identical to that used in the early work by Drell and Hiida[4] and by Deck.[4] We have not included such refinements of the model as pion Reggeization[5] or final-state rescattering (absorption).[12] We may expect this simple model to suffer to some extent from the diseases which these refinements are designed to cure, e.g., threshold enhancements which are too broad, and mass-slope correlations and total cross sections which are quantitatively incorrect. The virtue of our present approach is, of course, its relative simplicity. Our emphasis will be on the structure of the amplitude as a function of the decay angles, $\Omega(\theta, \phi)$, in the πN rest frame. The angular distributions in the πN rest frame are relatively insensitive to absorption[13] when an average is made over $|t_1|$. Rather more significant changes in the decay angular distributions would be expected if we were to include resonance-production amplitudes and modify our Deck amplitudes by final-state interactions.[14] Both alter the phases and the proportion of different partial waves in the $N\pi$ system and thereby modify $d\sigma(M, t_1)/d\Omega$. In this article we focus on the unmodified Deck "background," leaving to a possible later publication the inclusion of resonances and final-state interactions.

III. BARYON EXCHANGE

In addition to the π-exchange Deck term discussed in Sec. II, it has been recognized for some time that baryon exchange and direct terms[4,7,9,10] [Figs. 1(b) and 1(c)] are present in principle. They have been ignored for a combination of reasons, all largely pragmatic: II alone seemed to work ra-

ther well on the average, the B and D terms involve off-shell baryons and their attendant ambiguities, spin effects may no longer be ignored, and, finally, the sum of B and D is small because their amplitudes tend to cancel. Detailed information on the decay angular distribution of the $N\pi$ system from the Fermilab[1] and ISR[2] data on $aN \to a(N\pi)$ demonstrates, however, that the pion-exchange term alone is inadequate. The data suggest that discrepancies may be due to the baryon-exchange terms.[6] We address this possibility here.

There are two Deck-model contributions to the process $aN \to a(\pi N)$ which involve virtual nucleons; they are shown in Figs. 1(b) and 1(c). From a Feynman-graph point of view, it is clear that one should calculate both these diagrams and add the amplitudes. The direct-channel nucleon N in Fig. 1(c) is an off-shell nucleon, *not* a baryon resonance.

The ingredients of the N-exchange amplitude Fig. 1(b) are the following: (1) a propagator for the virtual nucleon which we generalize slightly from the Feynman propagator, $(\not{Q}_2 - m)^{-1}$, by allowing an additional term, $(\not{Q}_2 + m)^{-1}$, which has zero residue at the nucleon pole, (2) a $\pi\pi N$ vertex factor $ig\gamma_5$, (3) two form factors, $F_+(u_2)$ and $F_-(u_2)$, one for each term in the propagator, (4) an invariant amplitude $\mathfrak{M}_{Na}$ for the diffractive process $Na \to Na$, with the initial nucleon off the mass shell. The baryon-exchange contribution to $aN \to a(\pi N)$, then, has invariant amplitude

$$\mathfrak{M}_B = \bar{u}(p_2')\mathfrak{M}_{Na}(s_{12})\frac{F_+^B(u_2)(\not{Q}_2 + m) + F_-^B(u_2)(\not{Q}_2 - m)}{u_2 - m^2} \times i\sqrt{2}\, g\gamma_5 u(p_2)\,, \tag{3.1}$$

with m the nucleon mass. In most of the calculations to be presented, we use the simple Feynman propagator, $(\not{Q}_2 - m)^{-1}$. For this case the form factors are

$$F_+^B(u_2) = \exp(-\tfrac{1}{2}b_N^B|u_2 - m^2|), \qquad F_-^B(u_2) = 0. \tag{3.2}$$

In the Appendix we discuss how F_+ and F_- may be chosen differently so as to control the spin-parity content of the propagator.

The amplitude for the direct graph, Fig. 1(c), can be constructed in the same way:

$$\mathfrak{M}_D = \bar{u}(p_2')i\sqrt{2}\, g\gamma_5 \frac{F_+^D(s_2)(\not{q}_2 + m) + F_-^D(s_2)(\not{q}_2 - m)}{s_2 - m^2} \times \mathfrak{M}_{Na}(s)\, u(p_2)\,. \tag{3.3}$$

The form factors for this graph, F_+^D and F_-^D, may be different from F_+^B and F_-^B, since the nucleon is now timelike instead of spacelike. For the calculations with a Feynman propagator, we use

$$F_+^D(s_2) = \exp(-\tfrac{1}{2}b_N^D|s_2 - m^2|), \qquad F_-^D(s_2) = 0. \tag{3.4}$$

The invariant amplitude $\mathfrak{M}_{Na}$ is constructed using the same simplifying assumptions as in Sec. II. The spin of a is considered an unnecessary complication at large s, and the off-mass-shell corrections are assumed to be small. However, the structure of the amplitude in the nucleon (N) spin is a crucial issue, since we wish to study angular distributions in the low-mass πN rest frame, which is moving slowly with respect to the incident and final nucleons in the reaction. Since we ignore the quantum numbers of a, considering only Pomeron exchange, we may use the familiar formalism of πN scattering and write

$$\mathfrak{M}_{Na}(s) = A(s,t_1) + B(s,t_1)\not{P}, \tag{3.5}$$

with

$$P = (p_1 + p_1')/2.$$

We consider in detail two special cases of the spin structure of the amplitude for aN(offshell) to aN scattering. If it is s-channel helicity conserving (model s),

$$B_s(s,t_1) = i\sigma_{Na}\exp(\tfrac{1}{2}b_{Na}t_1), \tag{3.6}$$

and

$$A_s(s,t_1) = mB_s. \tag{3.7}$$

If it is t-channel helicity conserving (model t),

$$B_t(s,t_1) = 0, \tag{3.8}$$

and

$$A_t(s,t_1) = i\frac{s}{2m}\sigma_{Na}\exp(\tfrac{1}{2}b_{Na}t_1). \tag{3.9}$$

At $t_1 = 0$, both of these assumptions provide identical results. For $|t_1| > 0$, differences arise which are reflected in the decay angular distributions in the πN rest frame. Our normalizations in Eqs. (3.6) and (3.9) are fixed by the requirement that both choices lead to the same spin-averaged aN total cross section, σ_{Na}, at large s.

IV. SPIN SUMS

The amplitudes for π exchange (Π), baryon exchange (B), and direct production (D) expressed by (2.1), (3.1), and (3.3) must be added coherently, squared, summed over spins, and integrated over suitable kinematic variables. We use trace techniques to evaluate the spin sums associated with the six contributions to the squared amplitude,

$$|\Pi + B + D|^2 = |\Pi|^2 + |B|^2 + |D|^2 + 2(BD + \Pi D + B\Pi). \tag{4.1}$$

If, for both B and D, we define

$$F_1 = F_+ + F_-, \tag{4.2}$$

$$F_2 = F_+ - F_-, \tag{4.3}$$

and denote the arguments of the form factors and of the invariant amplitudes by a superscript [e.g., $F_1^B \equiv F_1(u_2)$, $A^B \equiv A(s_{12}, t_1)$], then the appropriate traces are

$$T^B = -\mathrm{Tr}[(\not{p}_2' + m)(A^B + B^B \not{P})(F_1^B \not{Q}_2 + F_2^B m)\gamma_5 \times (\not{p}_2 + m)\gamma_5 (F_1^B \not{Q}_2 + F_2^B m)(A^{B*} + B^{B*} \not{P})], \tag{4.4}$$

$$T^D = -\mathrm{Tr}[(\not{p}_2' + m)\gamma_5 (F_1^D \not{q}_2 + F_2^D m)(A^D + B^D \not{P}) \times (\not{p}_2 + m)(A^{D*} + B^{D*} \not{P})(F_1^D \not{q}_2 + F_2^D m)\gamma_5], \tag{4.5}$$

$$T^{BD} = -\mathrm{Tr}[(\not{p}_2' + m)(A^B + B^B \not{P})(F_1^B \not{Q}_2 + F_2^B m)\gamma_5 \times (\not{p}_2 + m)(A^{D*} + B^{D*} \not{P})(F_1^D \not{q}_2 + F_2^D m)\gamma_5], \tag{4.6}$$

$$T^{B\Pi} = -\mathrm{Tr}[(\not{p}_2' + m)\gamma_5 (\not{p}_2 + m)(A^{D*} + B^{D*} \not{P}) \times (F_1^D \not{q}_2 + F_2^D m)\gamma_5], \tag{4.7}$$

$$T^{B\Pi} = -\mathrm{Tr}[(\not{p}_2' + m)(A^B + B^B \not{P})(F_1^B \not{Q}_2 + F_2^B m)\gamma_5 \times (\not{p}_2 + m)\gamma_5]. \tag{4.8}$$

These traces must be multiplied by suitable propagators and vertex factors in order to calculate cross sections:

$$|B|^2 = \frac{1}{2}\frac{2g^2}{(u_2 - m^2)^2} T^B, \tag{4.9}$$

$$|D|^2 = \frac{1}{2}\frac{2g^2}{(s_2 - m^2)^2} T^D, \tag{4.10}$$

$$2BD = \frac{2g^2}{(u_2 - m^2)(s_2 - m^2)} T^{BD}, \tag{4.11}$$

$$2\Pi D = \frac{2g^2}{(s_2 - m^2)(t_2 - \mu^2)} \mathrm{Re}(T^{\Pi D} \mathfrak{M}_{\pi a}^*), \tag{4.12}$$

$$2B\Pi = \frac{2g^2}{(u_2 - m^2)(t_2 - \mu^2)} \mathrm{Re}(T^{B\Pi} \mathfrak{M}_{\pi a}^*). \tag{4.13}$$

The traces may be evaluated on a computer using the algebraic manipulation program ASHMEDAI.[15] The resulting expressions involve many terms in general. We have used these lengthy complete expressions for computation because, as we remark shortly, there is a large cancellation between B and D. We conjectured that nonasymptotic terms in these amplitudes might become anomalously important due to this cancellation. In fact, however, the leading-order terms in s and s_{12} yield angular distributions and total cross sections accurate to 10% at 10 GeV/c laboratory momentum and to 3% at 100 GeV/c. The asymptotic expressions below are entirely adequate.

For s-channel helicity-conserving diffractive amplitudes (model s), the traces yield the following asymptotic forms:

$$T_s^B = |B_s|^2\{[2s_{12}(u_2 - m^2)(s_{12} - s) - 2\mu^2 s_{12}^2](F_+^B + F_-^B)^2 + 8m^2 s_{12}[(s_{12} - s)F_+^B + s_{12}F_-^B]F_-^B\}, \tag{4.14}$$

$$T_s^D = |B_s|^2\{[2s(s_2 - m^2)(s - s_{12}) - 2\mu^2 s^2](F_+^D + F_-^D)^2 + 8m^2 s[(s - s_{12})F_+^D + sF_-^D]F_-^D\}, \tag{4.15}$$

$$T_s^{BD} = |B_s|^2(\{(s^2 + s_{12}^2)(t_1 - 4m^2) - 2ss_{12}(t_2 - m^2) - (s + s_{12})[s(u_2 - m^2) + s_{12}(s_2 - m^2)]\}F_1^B F_1^D + 4m^2(s^2 F_2^B F_1^D + s_{12}^2 F_1^B F_2^D) - 2m^2 s s_{12} F_2^B F_2^D), \tag{4.16}$$

$$T_s^{\Pi D} = \mathrm{Im}B_s\{[(s_2 - m^2)(s - s_{12}) - s(t_2 + \mu^2) + s_{12}t_1](F_+^D + F_-^D) + 4m^2(s - s_{12})F_-^D\}, \tag{4.17}$$

$$T_s^{B\Pi} = \mathrm{Im}B_s\{[(u_2 - m^2)(s_{12} - s) - s_{12}(t_2 + \mu^2) + st_1](F_+^B + F_-^B) + 4m^2(s_{12} - s)F_-^B\}. \tag{4.18}$$

Note that the mass of the a does not appear in these asymptotic expressions; the nonasymptotic terms (which we will not display) do depend on m_a.

The traces for model t are

$$T_t^B = |A_t^B|^2\{2[\mu^2(t_1 - 4m^2) - (s_2 - m^2)(u_2 - m^2)](F_+^B + F_-^B)^2 + 8m^2(t_2 + \mu^2 - t_1)F_+^B F_-^B - 8m^2(t_1 - \mu^2)(F_-^B)^2\}, \tag{4.19}$$

$$T_t^D = |A_t^D|^2\{2[\mu^2(t_1 - 4m^2) - (s_2 - m^2)(u_2 - m^2)](F_+^D + F_-^D)^2 + 8m^2(t_2 + \mu^2 - t_1)F_+^D F_-^D - 8m^2(t_1 - \mu^2)(F_-^D)^2\}, \tag{4.20}$$

$$T_t^{BD} = \mathrm{Re}A_t^{D*}A_t^B\{2[t_1\mu^2 - (u_2 - m^2)(s_2 - m^2)]F_1^B F_1^D + 4m^2(t_2 - \mu^2 - t_1)(F_+^B F_-^D + F_-^B F_-^D) - 8m^2(t_1 F_-^B F_-^D + \mu^2 F_+^B F_+^D)\}, \tag{4.21}$$

$$T_t^{\Pi D} = \mathrm{Im}A_t^D[2m(t_1 + \mu^2 - t_2)(F_+^D - F_-^D) + 4m(t_1 F_-^D - \mu^2 F_+^D)], \tag{4.22}$$

$$T_t^{B\Pi} = \mathrm{Im}A_t^B[2m(t_1 + \mu^2 - t_2)(F_+^B - F_-^B) + 4m(t_1 F_-^B - \mu^2 F_+^B)]. \tag{4.23}$$

Expressions (4.19)–(4.23) are exactly equal to the traces defined in (4.4) through (4.8). There are no terms of lower power in s for model t. It is a simple matter to verify that, when $t_1 \to 0$, $T_t^D(s_2 = m^2) = T_s^D(s_2 = m^2)$, as should be the case. Likewise, when $t_1 \to 0$, $T_t^B(u_2 = m^2) = T_s^B(u_2 = m^2)$. However, when the nucleons are off the mass shell ($s_2 > m^2$ or $u_2 < m^2$) and/or $t_1 \neq 0$, there are important differences between the t- and s-channel sets of amplitudes.

To calculate the cross section we include appropriate flux and phase-space factors:

$$\sigma = \frac{1}{4 p_{1\mathrm{ab}} m (2\pi)^5} \int \frac{d^3 p_1' d^3 p_2' d^3 k}{(2E_1')(2E_2')(2E_k)} \times \delta^4(Q) \left| \Pi + B + D \right|^2 . \tag{4.24}$$

where $Q = p_1 + p_2 - p_1' - p_2' - k$. Standard Monte Carlo techniques are used to evaluate the phase-space integral.

V. CANCELLATION

We present most of our computations for the reaction $pn \to p(\pi^- p)$ at $p_{1\mathrm{ab}} = 100$ GeV/c. Cross sections for $pp \to p(n\pi^+)$ may be obtained by multiplying our results by a factor of two. In model s and model t we specify parameters by the πN and NN total cross sections and elastic slopes,

$$(\sigma_{\pi N}, b_{\pi N}) = (24\ \mathrm{mb}, 8\ \mathrm{GeV}^{-2}), \tag{5.1}$$

$$(\sigma_{NN}, b_{NN}) = (40\ \mathrm{mb}, 10\ \mathrm{GeV}^{-2}), \tag{5.2}$$

and the form-factor parameters b_π, b_N^B, and b_N^D. We tried various values for b_π and found that the data are reproduced adequately with $b_\pi = 4\ \mathrm{GeV}^{-2}$. Although presently we will allow b_N^B to differ from b_N^D, for simplicity we now set both to the same value, $b_N^B = b_N^D = 2\ \mathrm{GeV}^{-2}$, and denote both by b_N.

A basic observation about the amplitudes of Sec. III is that the two diagrams, baryon exchange (B) and direct production (D), tend to cancel[4,16] so that

$$\mathfrak{M}_B + \mathfrak{M}_D \approx 0. \tag{5.3}$$

If spin factors are ignored, the amplitudes have the form

$$\mathfrak{M}_B \propto \frac{\exp[\frac{1}{2} b_N (u_2 - m^2)]}{u_2 - m^2}, \tag{5.4}$$

$$-\mathfrak{M}_D \propto \frac{\exp[\frac{1}{2} b_N (m^2 - s_2)]}{m^2 - s_2}. \tag{5.5}$$

However, u_2 and s_2 are related kinematically by

$$(u_2 - m^2) = (m^2 - s_2) - (t_2 - \mu^2) + t_1. \tag{5.6}$$

Since the diffractive amplitude, $\mathfrak{M}_{Na}$, constrains t_1 to be small, it is clear that (5.4) and (5.5) are identical for small t_2. The same equation (5.6) shows, more generally, that the Π, B, and D amplitudes cancel in pairs; e.g., for small t_1 and u_2 near m^2, the π-exchange and direct graph D cancel.

Because the spin factors are not the same for B and D and because we must average over t_1 and t_2, the cancellations are not exact. In Fig. 2 we show the contributions of the component amplitudes to $d\sigma/dt_2$ for model t. The cancellation of B and D is shown, as well as how $(B+D)$ combines with Π to give the total result. The extent of the cancellation is extraordinary at small $|t_2|$. The coherent sum $|B+D|^2$ is less than 5% of the peak value of the incoherent sum ($|B|^2 + |D|^2$), and the contribution from these graphs to the cross section is a small correction to the dominant π-exchange diagram. The pion-exchange term $|\Pi|^2$ is important even in that part of phase space closest to the baryon-exchange pole. For example, at $u_2 \simeq +0.4\ \mathrm{GeV}^2$, where $d\sigma/du_2$ has its maximum, we find that the ratio $|\Pi|^2$/total is approximately 0.65 in both model t and model s. For many purposes the traditional π-exchange Deck model is adequate.

The contribution from $(B+D)$ is concentrated in a specific kinematic region and materially affects the angular distributions in the πN rest frame in spite of the cancellation. We may define the decay angles of the πN system with respect to either the s-channel or the t-channel axes, as shown in Fig. 3. If the reaction proceeds in such a way that the helicity of the outgoing πN system is the same as that of the incoming N in the s channel (t channel), then the angular distribution $d\sigma/d\phi_s$ ($d\sigma/d\phi_t$) will be isotropic. This is the usual sense of the terms s-

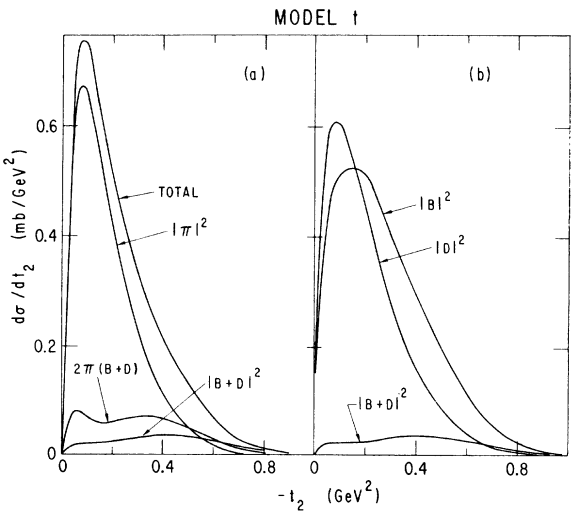

FIG. 2. Model-t cross section $d\sigma/dt_2$ for $np \to (p\pi^-)p$ at $p_{\mathrm{lab}} = 100$ GeV/c, $M < 1.4$ GeV, $0.02 < -t_1 < 1.0\ \mathrm{GeV}^2$. Shown in (a) is the net result ("total") as well as the three components which are added to obtain the total. In (b) the cancellation between the direct- and baryon-exchange terms is illustrated.

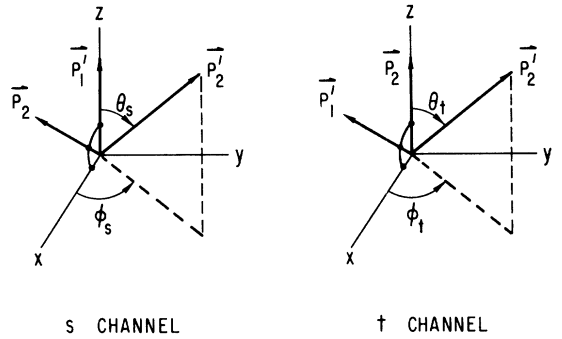

FIG. 3. Definition of the s-channel and t-channel decay angles of the πN system. The angles are all defined in the πN rest frame. Note that our conventions for defining these angles differ from those of Ref. 1.

channel and t-channel helicity conservation in diffraction dissociation. We belabor this point because we use these terms here in a different sense. When we speak of s-channel or t-channel helicity conservation, we refer to the helicity structure of the aN elastic diffractive amplitude Eq. (3.5), which is a component of the model.

We display in Figs. 4–6 the distributions in $\cos\theta_t$, ϕ_t, and ϕ_s for model t and model s. We select the region $M \leq 1.35$ GeV, where no strong resonance signals are seen in the experimental mass spectra. In Fig. 4 we compare $|B|^2$, $|D|^2$, and the coherent sum $|B+D|^2$. It is interesting that the two models are very different for $|B|^2$ and $|D|^2$ separately, but are quite similar for $|B+D|^2$. For model t we show in Fig. 5 how $(B+D)$ combines with Π to form the net cross section. Comparing the total to $|\Pi|^2$, one sees that the new graphs have sharpened the forward peak and have added a backward peak in the $\cos\theta_t$ distribution. An enhancement has also appeared for ϕ_s near π. The sharpened forward peak in $\cos\theta_t$ is in better agreement with data than that provided by π exchange alone, as is described in more detail in Sec. VI. While this may be regarded as a success of the inclusion of baryon exchange, we accept the improved agreement with some reservation. It would perhaps be preferable not to depend on the influence of the baryon contributions in that part of phase space ($\cos\theta_t \to +1$), where the pion term should be and is dominant.

It has been pointed out on general grounds[6,7] that peaks in the distribution $d\sigma/d\phi_s$ near $\phi_s = \pi$ are a signal of baryon exchange. Our explicit calculations here provide a numerical demonstration of how important such effects may be.

The modifications resulting from the addition of $(B+D)$ are much stronger for model s, as shown in Fig. 6; $d\sigma/d\cos\theta_t$ becomes strongly peaked backward, and $d\sigma/d\phi_s$ is almost as large at $\phi_s = \pi$ as at

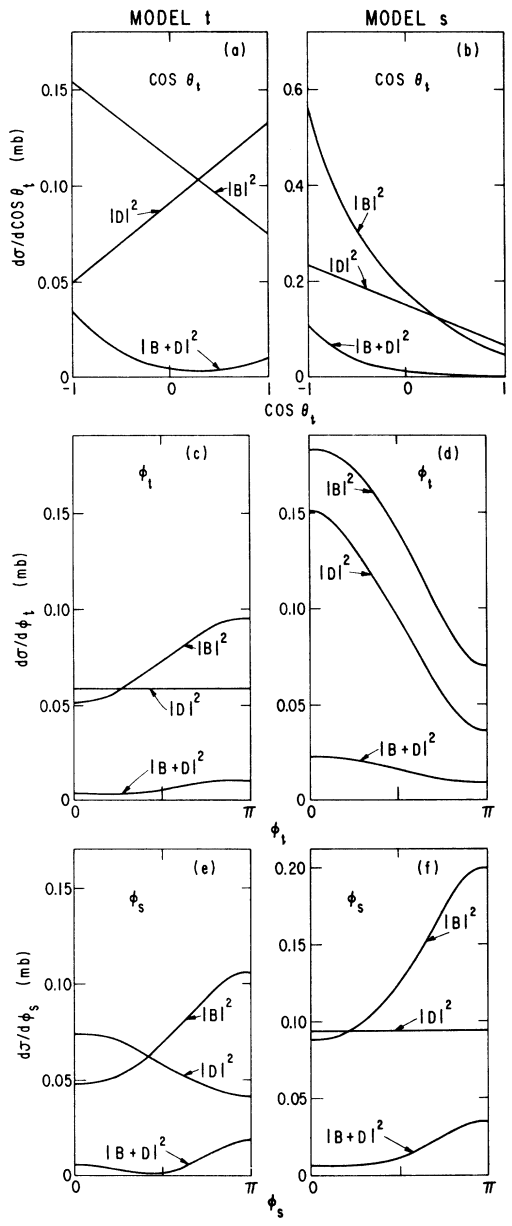

FIG. 4. Model-t and model-s distributions in $\cos\theta_t$, ϕ_t, and ϕ_s, showing the cancellation of B and D. The models are calculated for $np \to (p\pi^-)p$ at $p_{\text{lab}} = 100$ GeV/c, $M < 1.4$ GeV, and $0.02 < -t_1 < 1.0$ GeV^2.

$\phi_s = 0$. We will show in Sec. VI that model s does not agree with data as well as model t. Figures 5 and 6 show that the differences between model s and model t are due primarily to the interference term, $2\Pi(B+D)$. In model s this term is negative for $\cos\theta_t \approx 1$ and positive for $\cos\theta_t \approx -1$, producing the large backward peak in this angular distribution. The origin of this behavior can be identified if we examine the approximate forms of (4.12) and

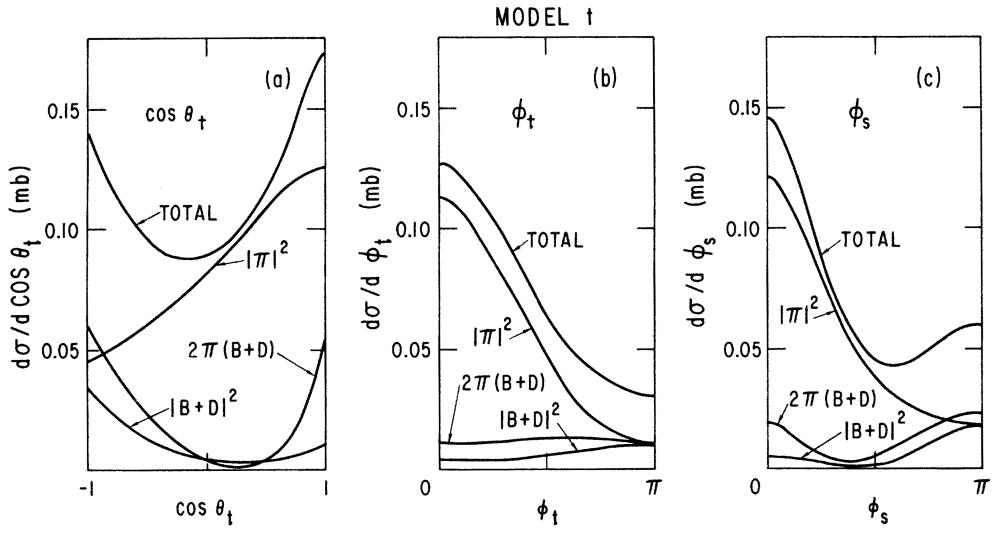

FIG. 5. Model-t distributions in $\cos\theta_t$, ϕ_t, and ϕ_s, showing how $(B+D)$ combines with Π. The model is calculated for $np \to (p\pi^-)p$ at $p_{\rm lab} = 100$ GeV/c, $M < 1.4$ GeV, $0.02 < -t_1 < 1.0$ GeV^2.

(4.13). If $b_N^B = b_N^D = b_N$, then (5.6) implies that

$$F_+^B = \exp[-\tfrac{1}{2}b_N(t_2 - t_1 - \mu^2)]F_+^D. \tag{5.7}$$

For $\cos\theta_t \approx -1$ and t_1 small, $(t_2 - t_1)$ is negative and

$$F_+^B > F_+^D, \quad \cos\theta_t \approx -1. \tag{5.8}$$

Thus, the $B\Pi$ term is favored over ΠD, and dropping terms proportional to μ^2, we derive

$$B\Pi \propto \frac{F_+^B[(s_{12}-s)(u_2-m^2)+st_1]}{(u_2-m^2)t_2}, \tag{5.9}$$

which is positive for small t_1.

In the forward direction,

$$F_+^B \approx F_+^D, \quad \cos\theta_t \approx 1, \tag{5.10}$$

and

$$\Pi(B+D) \propto \frac{(s_{12}-s)(t_1+t_2)}{t_2(s_2-m^2)}F_+, \tag{5.11}$$

which is negative.

This discussion suggests that the unwanted positive interference contribution near $\cos\theta_t = -1$ may not occur if the form-factor slope b_N^B is larger than b_N^D. In fact, the agreement of model s with data is

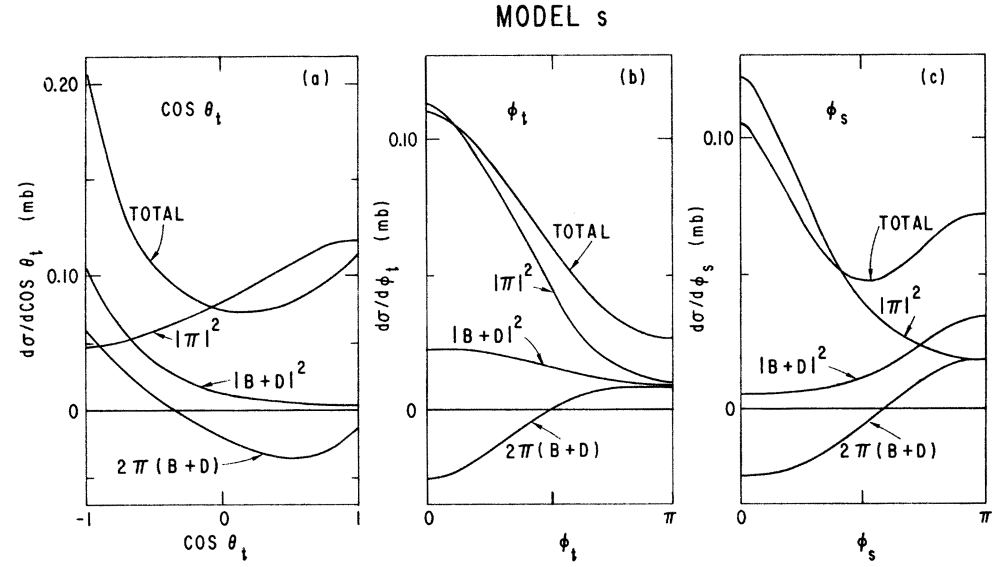

FIG. 6. Model-s distributions in $\cos\theta_t$, ϕ_t, and ϕ_s, showing how $(B+D)$ combines with Π. The model is calculated for $np \to (p\pi^-)p$ at $p_{\rm lab} = 100$ GeV/c, $M < 1.4$ GeV, $0.02 < -t_1 < 1.0$ GeV^2.

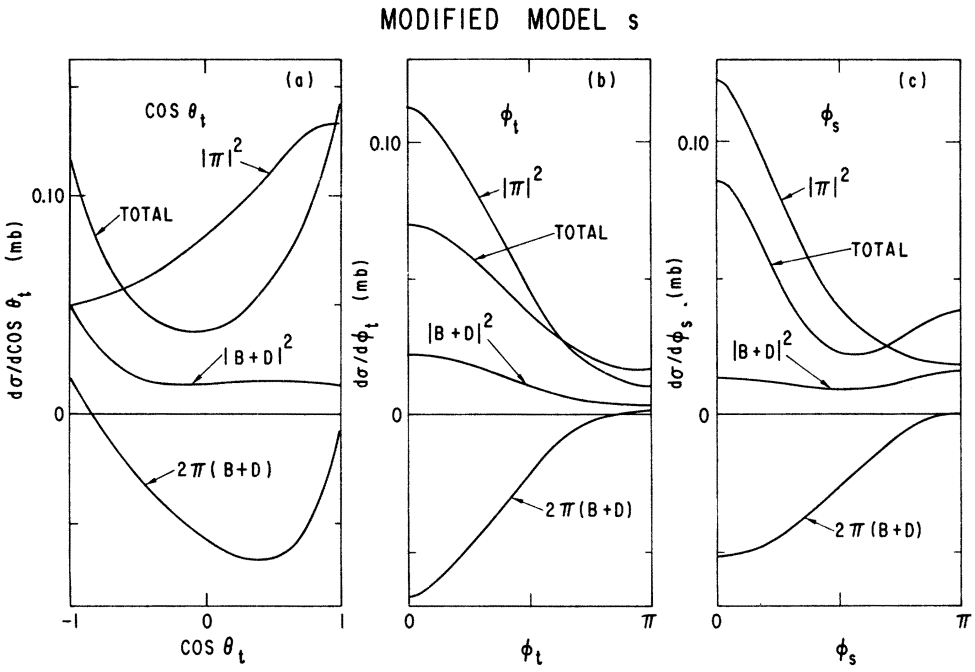

FIG. 7. Modified-model-s distributions in $\cos\theta_t$, ϕ_t, and ϕ_s, showing how $(B+D)$ combines with Π. The model is calculated for $np \to (p\pi^-)p$ at $p_{\rm lab} = 100$ GeV/c, $M < 1.4$ GeV, $0.02 < -t_1 < 1.0$ GeV^2.

improved greatly if we set $(b_N^D, b_N^B) = (2\ \text{GeV}^{-2}, 3\ \text{GeV}^{-2})$. We denote this choice of form factors "modified model s" and show in Fig. 7 how the interference term, which is now entirely negative, affects the angular distributions.

VI. COMPARISON WITH DATA

We compare model t, model s, and modified model s to the data of Ref. 1 on $pn \to p(p\pi^-)$. The ISR data on $pp \to pn\pi^+$ are qualitatively similar.[2] We fix $p_{\rm lab} = 100$ GeV/c for most of our computations. In order to avoid as much as possible the obvious resonancelike effects in the data, the $p\pi^-$ mass is restricted to $M < 1.35$ GeV. The total cross sections for $M < 1.35$ GeV and $0.02 < -t_1 < 1.0$ GeV^2, calculated from the models (s, t, modified s), are (190 μb, 160 μb, 100 μb). These cross sections are a factor of two to three larger than the experimental value of 59 ± 6 μb. Similar overestimates are encountered in other Deck-model calculations of nucleon dissociation.[17] The contribution from $|\Pi|^2$ alone is 140 μb. In Fig. 8 we display the energy dependence of our model-s cross section for $M < 1.4$ GeV and $0.02 < |t_1| < 1.0$ GeV^2. Our full model t and the term $|\Pi|^2$ representing the pion-exchange term alone provide essentially the same s dependence as the model s shown in Fig. 8. Even though our amplitude is purely diffractive, we compute a decrease of σ by a factor of 2 as $p_{\rm lab}$ increases from 5 to 100 GeV/c. At least half of this decrease is purely kinematic in origin. The amplitude $s_1/(\mu^2 - t_2)$ is proportional to $s/(M^2 - m^2)$ at small t_1. Thus, $\sigma \propto s^2 \times$ (phase space)/flux $\sim (s/p_{\rm lab})^2$. The energy dependence of $(s/p_{\rm lab})^2$ is also shown in Fig. 8. Above $p_{\rm lab} = 100$ GeV/c, our calculated cross sections are essentially constant.

The t_1 dependence of models t and s is compared with data in Fig. 9. The theoretical curves are normalized to the integrated data for all $\cos\theta_t$ in Fig. 9(a). The normalizations in Figs. 7(b)–7(d) are then predicted. When no selections are made

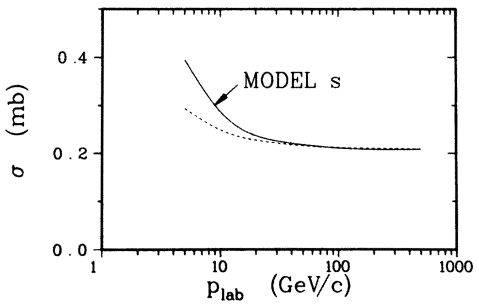

FIG. 8. Calculated cross section as a function of laboratory momentum for model s (solid curve) for $np \to (p\pi^-)p$ with $M < 1.4$ GeV and $0.02 < -t_1 < 1.0$ GeV^2. For comparison we show as a dashed curve the energy dependence of the ratio $(s/p_{\rm lab})^2$. The energy dependences are essentially identical for model t and for the pion-exchange term $|\Pi|^2$.

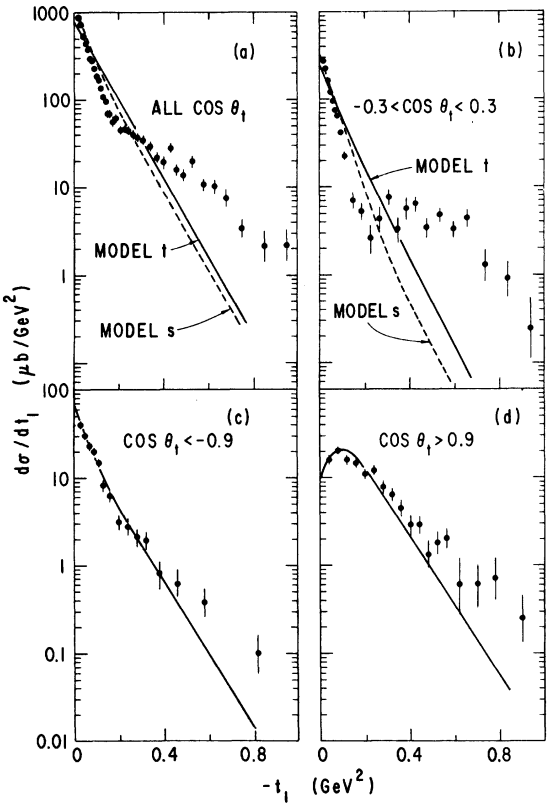

FIG. 9. Distributions in t_1 for $np \to (p\pi^-)p$ at $p_{\rm lab}$ = 100 GeV/c and $M < 1.35$ GeV. The solid theoretical curves are computed from model t and are multiplied by 0.32 in order to make the integrated cross section agree with data. Dashed lines show results of model s scaled by 0.37. The data are from Ref. 1.

on $\cos\theta_t$, Fig. 9(a), the models are at variance with the data. The data fall off more steeply than theory for small t_1 and display a break at about $t_1 = -0.2$ GeV^2. These experimental features are enhanced in the central region of $\cos\theta_t$, Fig. 9(b), where our present unabsorbed model fails badly. The t_1 dependence of model t is in adequate agreement with data for $\cos\theta_t$ near both the forward and backward kinematic boundaries, as shown in Fig. 9(c) and Fig. 9(d). Results for model s are not plotted in Figs. 9(c) and 9(d); they are almost identical to those of model t in these regions of $\cos\theta_t$. The forward turnover evident in Fig. 9(d) for $\cos\theta_t > 0.9$ and $|t_1| < 0.2$ GeV^2 is reproduced well. It originates from the $(-t_2)^{1/2}$ factor in the pion-exchange Deck amplitude Eq. (2.4). For $\cos\theta_t < -0.9$, a sharpening of the t_1 distribution is evident below $|t_1| \simeq 0.2$ GeV^2 in Fig. 9(c). A consequence of our baryon-exchange term, this low-$|t_1|$ feature appears naturally in our model without absorption.

We may define the logarithmic slope, b, of our calculated spectra by fitting our results to the

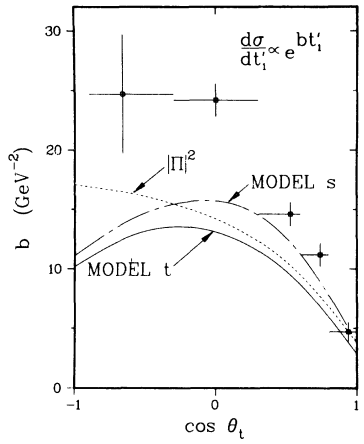

FIG. 10. Logarithmic slope b of the momentum-transfer distribution $d\sigma/dt_1'$ is shown as a function of the decay angle $\cos\theta_t$. The mass range selected is $1.30 \leq M \leq 1.35$ GeV. The data are from Ref. 2.

form $d\sigma/dt_1' = A \exp(bt_1')$, where A is a constant (which depends on $\cos\theta_t$). In Fig. 10 we compare our values of b with those published by the CHOV ISR group.[2] The values of b were obtained from a fit over the range $0 < |t_1'| < 0.2$ GeV^2. Our model s agrees quite well with the ISR data for $\cos\theta_t \gtrsim 0.4$. The discrepancy for $\cos\theta_t \simeq 0$ was mentioned above. For $\cos\theta_t \to -1$, our comparison with Fermilab data in Fig. 9(c) shows good agreement, whereas we appear to fall below the ISR results in Fig. 10. Because of experimental acceptance limitations, the ISR data are not altogether reliable near $\cos\theta_t = -1$.

The failure of the unabsorbed Deck model to reproduce the experimental structure near $|t_1| = 0.2$ GeV^2 for the central decay angles, $|\cos\theta_t| < 0.3$, has no clear interpretation as yet. As remarked in the Introduction, one view is that absorptive effects are required. While these lead naturally to peripheral structure in t_1 distributions, it is usually difficult to produce dips at t_1 values as small as 0.2 GeV^2 without an increase (perhaps artificial) of the strength of the absorption. Fortunately, absorption should cause little change in Fig. 9(d), leaving the agreement with data unaffected, because its strength is usually small whenever the unabsorbed pole term vanishes near $t_1 = 0$. By contrast, absorption strong enough to reproduce Fig. 9(b) would tend to create a dip in Fig. 9(c) where none is observed. Instead of absorption, one may imagine that a second component, perhaps resonancelike, is involved in addition to the unabsorbed Deck contribution. If this second component is postulated to be of peripheral character in impact parameter and to dominate the πN decay angular distribution for $|\cos\theta_t| < 0.3$, the data could be "ex-

plained" in at least qualitative terms. In this latter viewpoint, the success of the Deck model for $|\cos\theta_t| \gtrsim 0.5$ is attributed to the dominance of the Deck component in these kinematic regions, and absorption, if any, is assigned a minor role. Separating the postulated two components is operationally difficult since they populate overlapping regions of phase space. Nevertheless, it is undeniable that resonancelike signals are visible in the data, and these are not incorporated in the Deck model. We shall return to this point in Sec. VII.

In Fig. 11 we compare our calculated slopes with data as a function of mass M. All models provide a "mass-slope correlation," such that b decreases as M increases, in qualitative agreement with the data.[18] A relatively mild decrease of b with M is present for $|\Pi|^2$ alone, and its origin is well understood theoretically.[6] The magnitude of b near threshold ($M = 1.08$ GeV) is increased markedly by the inclusion of the baryon terms in model s and in modified model s, whereas little change from $|\Pi|^2$ results in model t. The slope b computed from model s agrees with the data at threshold, but is roughly 5 units too small near $M = 1.3$ GeV. We showed above that this shortage is associated with the central decay angles, $\cos\theta_t \simeq 0$.

In Fig. 12 we show two-dimensional contour plots of the distribution $d\sigma/d\cos\theta_t d\phi_t$ for the three models and for $|\Pi|^2$ alone. All models show a large π-exchange peak near $(\cos\theta_t, \phi_t) = (1, 0)$ and a depleted region near $(0.5, \pi)$. These features are also strongly visible in scatter plots of the data.[1,2,3] Model s provides a greater population than the other models for $\cos\theta_t$ near -1, with a large peak near $(-1, 0)$. This latter structure is not present in the data, as we shall see. Modified model s also shows an enhancement near $(-1, 0)$, but it is less strong than that of model s. The depleted region centered on $(0.5, \pi)$ is larger in modified model s than in the other models.

We remark in passing that it is also possible to modify model s in a second way with the result that the angular distributions are virtually identical to those of model t [Fig. 12(a)]. This is done by choosing $b_N^B = b_N^D = 2$ GeV^{-2}, as in model t, but reducing the total cross section for virtual NN scattering to $\sigma_{NN} = 23$ mb. The cross section for $M < 1.35$ GeV and $0.02 < -t_1 < 1.0$ GeV^2 becomes 140 μb for this version of model s, somewhat less than the cross sections for model t (190 μb) or model s (160 μb).

Predicted decay spectra in the πN decay angles $\cos\theta_t$, ϕ_t, $\cos\theta_s$, and ϕ_s are shown in Figs. 13–15 for three ranges of t_1. Since we have already shown in Fig. 9 that our models do not reproduce $d\sigma/dt_1$ correctly for all $\cos\theta_t$, we normalize the integrated cross section of each curve to the data in Figs. 13–15. In Fig. 13 model t reproduces the experimental spectra to excellent accuracy in all four angular distributions and at both large and small $|t_1|$. In Fig. 14 we see that the expectations of model s for $\cos\theta_t$ and ϕ_s are in some disagree-

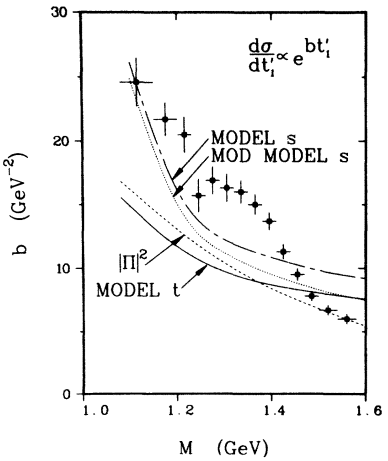

FIG. 11. Logarithmic slope b of the momentum-transfer t_1 dependence of model t, calculated for $np \to (p\pi^-)p$ at $p_{\rm lab} = 100$ GeV/c as a function of M, the $p\pi^-$ mass. The curves are obtained by fitting $d\sigma/dt_1' dM = A(M)\exp[b(M)t_1']$ over the range $0 < -t_1' < 0.2$ GeV^2 at various values of M. The data are from Ref. 1.

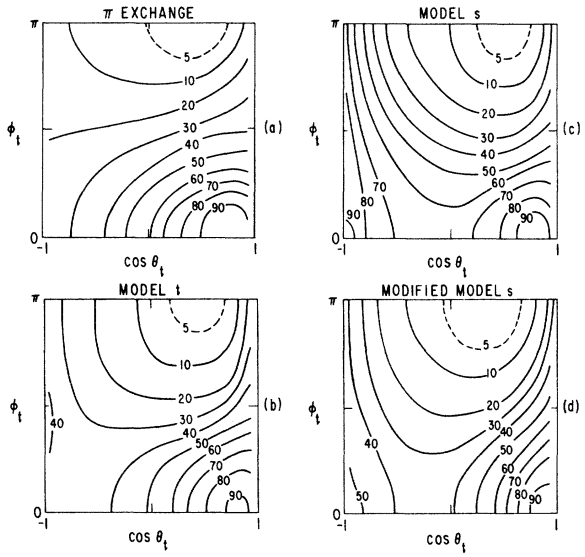

FIG. 12. Two-dimensional distributions in the variables ϕ_t and $\cos\theta_t$ for $np \to (p\pi^-)p$ at $p_{\rm lab} = 100$ GeV/c, $M < 1.35$ GeV, and $0.02 < -t_1 < 1.0$ GeV^2. The contours are labeled in percentage of the maximum value of $d\sigma/d\cos\theta_t d\phi_t$. Our convention for defining ϕ_t differs from that in Ref. 1; thus, our $\phi_t = \pi$ corresponds to $\phi_t = 0$ in Ref. 1.

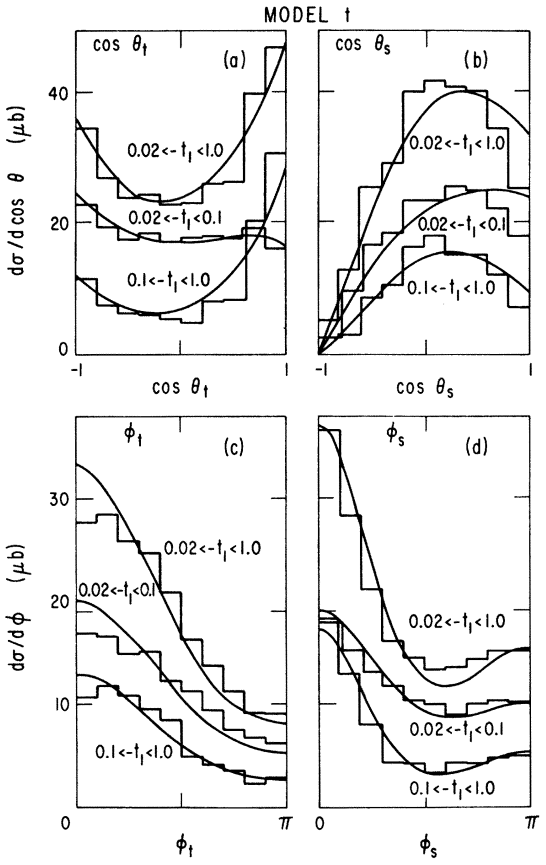

FIG. 13. Model-t distributions in t-channel and s-channel decay angles compared with Fermilab data (Ref. 1) for the reaction $np \to (p\pi^-)p$ at $p_{\rm lab} = 100$ GeV/c, $M < 1.35$ GeV for three ranges of t_1. Each curve is normalized to the data.

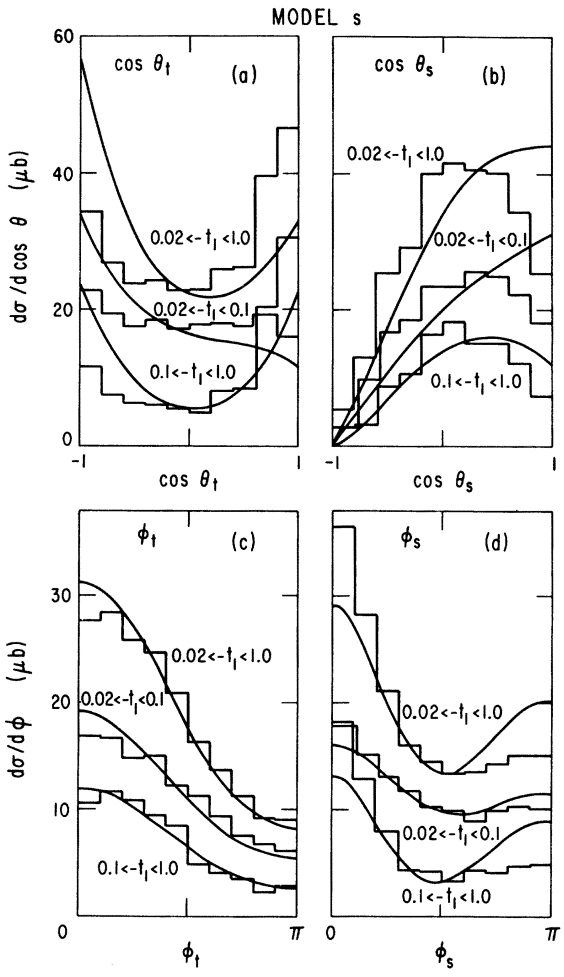

FIG. 14. Model-s distributions in t-channel and s-channel decay angles compared with Fermilab data (Ref. 1) for the reaction $np \to (p\pi^-)p$ at $p_{\rm lab} = 100$ GeV/c, $M < 1.35$ GeV, for three ranges of t_1. Each curve is normalized to the data.

ment with the data. The deviations are most apparent for $|t_1| > 0.1$ GeV^2, but are also visible for $|t_1| < 0.1$ GeV^2, where the s- and t-channel differences should be the least significant.

In Fig. 15 the modification to the form factors in model s reduces these discrepancies to modest proportions. The $\cos\theta_t$ distribution, Fig. 15(a), is still too small near $\cos\theta_t = 0$, but the ratio between forward and backward cross sections is approximately correct. These features are seen in both ranges of t_1.

As is clear in Fig. 12, model s differs most strikingly from model t and from modified model s in the region $\cos\theta_t \approx -1$. Accordingly, for $\cos\theta_t < -0.8$, we compare the ϕ_t spectra of these three models with data in Fig. 16, using the same normalizations for the theoretical curves as in Figs. 13–15. Model t is in reasonable accord with the data, but both versions of model s are too large near $\phi_t = 0$. The data may suggest some peaking towards $\phi_t = \pi$ when $-t_1 < 0.1$ GeV^2, an effect not present in the theory. For reasons discussed in Sec. VII, we do not consider this discrepancy to be terribly serious.

A few general comments are in order regarding Figs. 12–15. First, the baryon terms improve agreement with the data substantially. Second, it is evident that the spin-related effects are nontrivial in the model. Indeed, from a model for $np \to (p\pi^-)p$ in which the spin of the dissociating system is ignored,[1] a baryon-exchange peak is produced in the scatter plot Fig. 12 near $(\cos\theta_t, \phi_t) = (-1, \pi)$. No such peak is present in our models, and none is visible experimentally. Another technical aspect of spin dependence is discussed in the Appendix. Third, it would appear superficially that the data shown in Figs. 13–15 favor the assumption of t-channel helicity conservation for the off-shell

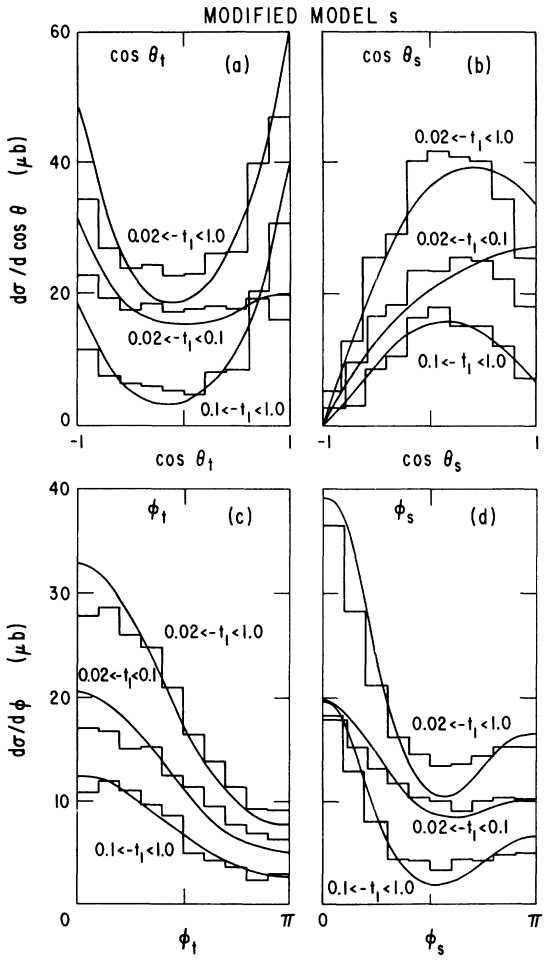

FIG. 15. Modified-model-s distributions in t-channel and s-channel decay angles compared with Fermilab data (Ref. 1) for the reaction $np \to (p\pi^-)p$ at p_{lab} = 100 GeV/c, M < 1.35 GeV, for three ranges of t_1. Each curve is normalized to the data.

to on-shell aN elastic scattering amplitude, rather than the usual preference for s-channel conservation in elastic scattering.[20] We believe this conclusion cannot be drawn for various reasons, including the uncertainties of off-shell extrapolation. We note that merely scaling down the size of the baryon-exchange amplitude in model s by approximately a factor of two is sufficient to restore agreement with data as good as is obtained with model t. We recall in this connection the notorious problems encountered with pole extrapolation (normalization) in πN backward elastic scattering[11] (also mediated by baryon exchange). Furthermore, minor adjustments to the form factor associated with a spacelike virtual nucleon (cf., modified model s) can have a large effect on these angular distributions. From the angular distributions alone, then, we can conclude nothing for or against s- or t-channel helicity conservation in the aN elastic amplitudes inbedded in Figs. 1(b) and 1(c). The slope values in Fig. 11 would suggest that s-channel helicity conservation is preferred. However, our inability to reproduce $d\sigma/dt_1$ for $\cos\theta_t \simeq 0$ weakens any conclusion to be drawn from slopes.

VII. CONCLUSIONS AND DISCUSSION

In a Drell-Deck-model description of high-energy nuclear diffraction dissociation, $aN \to a(N\pi)$, we have studied in detail the contributions which the baryon-exchange and direct-baryon-pole Deck graphs make to the production and decay distributions of the low-mass $N\pi$ system. Adopting reasonable parametrizations of these baryon terms, we show that their inclusion improves substantially the agreement of the model with the data on the $N\pi$ decay angular distributions $d\sigma/d\Omega(\theta, \phi)$, particularly in that region of phase space where the dominant π-exchange term is suppressed. In our parametrizations we considered both s- and t-channel conserving forms for the off-shell elastic NN amplitudes embedded in the inelastic Deck amplitudes. In part because of theoretical freedom in the treatment of off-shell baryons (including form factors), we are unable to conclude that the data favor either the s- or the t-channel version. Both are consistent with the data on $d\sigma/d\Omega$. The s-channel model is significantly better in one respect. It provides correctly the very large value (~25 GeV^{-2}) of the logarithmic slope b of $d\sigma/dt_1 dM_{N\pi}$ for $M_{N\pi}$ near threshold ($M_{N\pi}$ = 1.08 GeV). However, in both models, b is 25 to 40% below the experimental value for $M \sim 1.3$ GeV (Fig. 11). This slope discrepancy is associated with a failure of the model to reproduce the dip in the experimental $d\sigma/dt_1 dM$ near $t_1 = -0.2$ GeV^2, a feature of the data pronounced only near $\cos\theta_t = 0$. The model does well for $|\cos\theta_t| > 0.5$ (Fig. 9).

When structure is observed in a differential cross section $d\sigma/dt_1$ near $|t_1| = 0.2$ GeV^2, it is natural to postulate that absorptive effects are called for.[12] In this picture the structure is a property of one dominant non-spin-flip *amplitude*, a controversial hypothesis by no means obvious from the data. Moreover, on purely technical grounds, it is hard to imagine that absorption strong enough to produce the pronounced dip in $d\sigma/dt_1$ for $\cos\theta_t \simeq 0$ would not also distort $d\sigma/dt_1$ for $|\cos\theta_t| > 0.9$, where, as shown in Figs. 9(c) and 9(d), the unabsorbed model does well enough.

In our view there are several inadequacies of the model in addition to the problem with $d\sigma/dt_1$ which should not be ignored and whose effects are potentially more significant than those of absorption. In

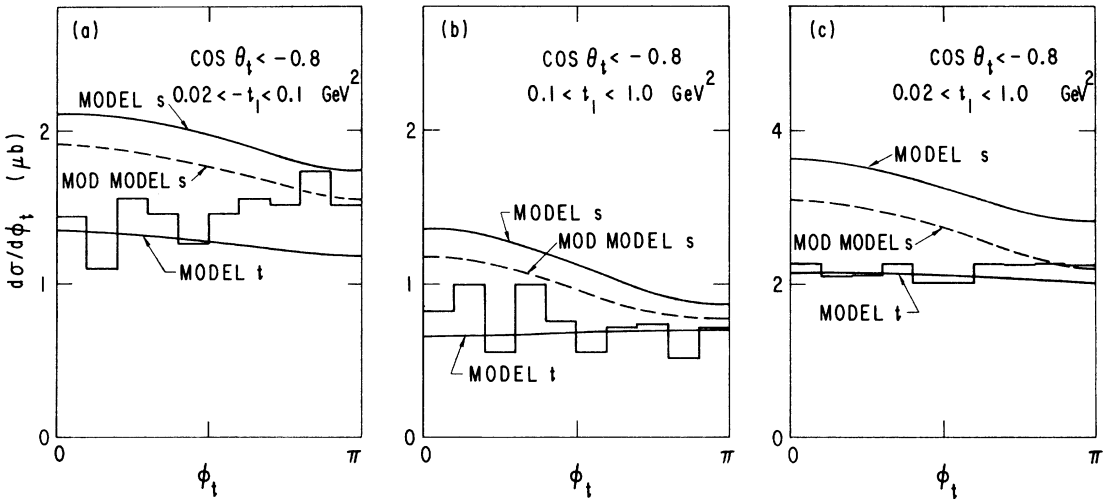

FIG. 16. The distribution $d\sigma/d\phi_t$ for $\cos\theta_t < -0.8$ for model s, model t, and modified model s compared with Fermilab data (Ref. 1) in three t_1 ranges. The reaction is $np \to (p\pi^-)p$ at $p_{\text{lab}} = 100$ GeV/c, $M < 1.35$ GeV.

comparison with data, the shape of $d\sigma/dM$ is woefully inadequate (e.g., no resonance peaks), and we predict too much cross section. On the theoretical side, as the model stands it does not have the correct unitarity and phase structure[14] as a function of the $N\pi$ mass. If we were to make a partial-wave decomposition of our Deck amplitudes in the final-state $N\pi$ channel, we would obtain essentially real partial-wave amplitudes $f^{J^P}_{\text{Deck}}(M, t_1)$. However, according to the Watson final-state-interaction theorem,[21] each wave should carry the phase $\delta^J(M)$ of πN elastic scattering. Furthermore, in addition to the Deck term, each resonant wave may be produced by a *direct* coupling to the exchanged Pomeron. The t_1 dependence of the direct-coupling term need bear no simple relationship to that of $f^{J^P}_{\text{Deck}}(M, t_1)$. It is not inconceivable that interference effects between the two would provide structure in $d\sigma/dt_1$ near $|t_1| = 0.2$ GeV^2 and/or that the peripheral structure seen in the data is a property of the direct coupling itself. It is reasonable to conjecture the final-state interactions and the addition of direct production will provide substantially modified differential angular distributions $d\sigma/d\Omega$ in the $N\pi$ rest frame. This may be true even for values of M in the region $M \simeq 1.2$ to 1.4 GeV, where no obvious resonance signals are visible in $d\sigma/dM$. We conclude that the discrepancies between our models and the data can reasonably be ascribed to our omission of final-state interactions, and that, given this limitation, we have done as well with our baryon-exchange terms as is reasonable to expect. While further gymnastics with the off-shell baryon propagators may appear seductive in attempts to improve agreement with selected features of the data, we consider the final-state-interaction approach more compelling.

Our work has features in common with calculations presented by Babaev *et al.*[3] and by Minaka, Sumiyoshi, and Uehara.[10] In both of these articles, baryon-exchange Deck models are presented and comparisons are made with recent data. Babaev *et al.* use an s-channel helicity-conserving diffractive amplitude and differ from our model s primarily in their choice of form factors. They claim that the Serphukov data[3] on $np \to (p\pi^-)p$ are in substantial agreement with their model, although they feel that absorptive corrections to the model are indicated. Minaka *et al.* consider both s-channel and t-channel helicity-conserving diffractive amplitudes and briefly discuss the possibility of modifying the baryon propagator with the form factor we call F_-. They treat the process $\pi N \to \pi(N\pi)$ and conclude that baryon-exchange Deck models cannot reproduce the angular dependence of the Fermilab-Rochester-Northwestern data.[1] We believe that our more detailed analysis of the model shows this conclusion to be incorrect. The sensitive nature of the cancellation between baryon-exchange and direct amplitudes leads to a situation where minor changes in the parametrizations of these amplitudes can have large effects on these angular distributions. The angular behavior of the data can be well reproduced with a suitable choice of parameters.

ACKNOWLEDGMENTS

We are indebted to members of the Rochester-Northwestern-Fermilab-SLAC collaboration, especially to J. Biel, for providing distributions of experimental data. Conversations with T. Ferbel, C. Broll, and J. Favier were also most helpful to

us. E.L.B. is grateful for the warm hospitality of the CERN Theoretical Studies Division where part of this work was carried out.

APPENDIX: MODIFIED BARYON PROPAGATOR

We considered various modifications to the off-shell baryon propagator in an attempt to estimate the sensitivity of our results to the parametrizations used. We report on one such exercise in this Appendix.

The form factors F_+ and F_- in the baryon propagator, introduced in Sec. III, allow the spin-parity content of the virtual baryon to be modified. To be specific, we consider the direct-channel graph, Fig. 1(c). (The form factors we find can then be used for the baryon-exchange graph as well). The baryon propagator is pure $J^P=\frac{1}{2}^+$ at the nucleon pole. Were it to remain a pure spin-parity state off the pole, the helicity-conserving model t, for example, would produce isotropic contributions in the πN decay angles $(\cos\theta_t, \phi_t)$. However, as is shown in Fig. 4(a), the contribution from the direct graph $|D|^2$ to the $\cos\theta_t$ distribution is not isotropic. The Feynman baryon propagator [$F_-=0$ in Eq. (3.1)] contains a mixture of $J^P=\frac{1}{2}^+$ and $\frac{1}{2}^-$ which interfere to give an angular dependence,

$$d\sigma/d\cos\theta_t \propto \sum_{\lambda'} \left|\left[1+\epsilon(-1)^{\lambda-\lambda'}\right] d_{\lambda\lambda'}{}^{1/2}(\theta_t)\right|^2 = (1+\epsilon^2)+\epsilon\cos\theta_t, \quad \text{(A1)}$$

where ϵ is the ratio of $\frac{1}{2}^-$ to $\frac{1}{2}^+$ in the propagator at a given M, λ is the incoming helicity.

To illustrate this matter in more detail, we consider the direct-channel graph for $\pi N \to \pi N$ shown in Fig. 17. Allowing the nucleon propagator the more general form involving F_+ and F_-, we write the amplitude for this reaction as

$$\mathfrak{M}_{\pi N}=\bar{u}(p_1')ig\gamma_5\frac{F_+(\not{q}+m)+F_-(\not{q}-m)}{s-m^2}ig\gamma_5 u(p_1) \quad \text{(A2)}$$

$$=\frac{g^2}{s-m^2}\bar{u}(p_1')[(F_++F_-)\not{p}_2+F_- 2m]u(p_1). \quad \text{(A3)}$$

The amplitude can be recast in terms of the invariant amplitudes A and B,

$$\mathfrak{M}_{\pi N}=\bar{u}(p_1')(A+B\not{p}_2)u(p_1). \quad \text{(A4)}$$

Comparing (A3) and (A4), one sees that

$$A=2mF_-\frac{g^2}{s-m^2}, \quad \text{(A5)}$$

$$B=(F_++F_-)\frac{g^2}{s-m^2}. \quad \text{(A6)}$$

Amplitudes of definite spin and parity can be formed as

$$f_{1/2^-}=\frac{E+m}{2\sqrt{s}}[A+(\sqrt{s}-m)B], \quad \text{(A7)}$$

$$f_{1/2^+}=\frac{E-m}{2\sqrt{s}}[-A+(\sqrt{s}+m)B], \quad \text{(A8)}$$

where E is the energy of the proton in the πN center-of-mass system. In terms of the form factors, we find

$$f_{1/2^+}\propto\frac{g^2}{s-m^2}[\sqrt{s}F_1+mF_2], \quad \text{(A9)}$$

$$f_{1/2^-}\propto\frac{g^2}{s-m^2}[\sqrt{s}F_1-mF_2], \quad \text{(A10)}$$

where

$$F_1=F_++F_-, \quad \text{(A11)}$$

$$F_2=F_+-F_-. \quad \text{(A12)}$$

These amplitudes, of course, satisfy the Mac-Dowell symmetry relation

$$f_{1/2^+}(\sqrt{s})=-f_{1/2^-}(-\sqrt{s}). \quad \text{(A13)}$$

The conditions on F_1 and F_2 necessary in order to have a propagator with a single spin parity are

$$f_{1/2^-}=0 \to F_2=\frac{\sqrt{s}}{m}F_1, \quad \text{(A14)}$$

$$f_{1/2^+}=0 \to F_=-\frac{\sqrt{s}}{m}F_1. \quad \text{(A15)}$$

These equations demonstrate that the analyticity in s of the invariant amplitudes A and B would have to be sacrificed in order to have a virtual baryon in a pure spin-parity state for all s. However, one can arrange that the propagator reduce to a single spin parity at one specific value of s, say $s_0=M_0^2$, without damage to analyticity. Since the propagator is pure $\frac{1}{2}^+$ at the pole, if we chose $F_1(s)$ and $F_2(s)$ so that

$$F_+(m^2)=\tfrac{1}{2}[F_1(m^2)+F_2(m^2)]=1, \quad F_-(m^2)=0, \quad \text{(A16)}$$

$$F_2(s_0)=\frac{\sqrt{s_0}}{m}F_1(s_0), \quad \text{(A17)}$$

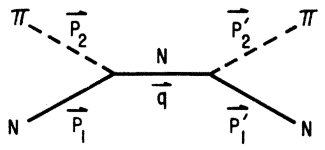

FIG. 17. Direct-channel graph for $\pi N \to \pi N$ used as a prototype for the Pomeron-nucleon interaction of Fig. 1(c), $PN \to \pi N$.

then the unnatural-parity contribution, $f_{1/2^-}$, will be zero at $s = s_0$. Moreover, it will be small for s not too different from s_0.

Thus motivated, we parametrize

$$F_1(s) = \exp(-\tfrac{1}{2} b_{N2} |s - m^2|), \quad \text{(A18)}$$

$$F_2(s) = \exp(-\tfrac{1}{2} b_{N1} |s - m^2|), \quad \text{(A19)}$$

with

$$b_{N1} = b_{N2} + \frac{2}{s_0 - m^2} \ln \frac{\sqrt{s}_0}{m}. \quad \text{(A20)}$$

To arrange that $J^P = \frac{1}{2}^+$ be dominant in the low-M region, we select

$$M_0 = \sqrt{s}_0 = 1.3 \text{ GeV}. \quad \text{(A21)}$$

Choosing

$$b_{N2} = 2 \text{ GeV}^{-2}, \quad \text{(A22)}$$

we obtain

$$b_{N1} = 2.8 \text{ GeV}^{-2}. \quad \text{(A23)}$$

Our choice of form factors yields a propagator which is primarily natural parity, $J^P = \frac{1}{2}^+$, for $M \lesssim 1.4$ GeV. As expected, when model t and model s are calculated, the contributions of $|D|^2$ to the contributions in $\cos\theta_t$ and in $\cos\theta_s$ are found to be almost isotropic for $M \leq 1.35$ GeV and our usual selections on $|t_1|$. The nucleon-exchange amplitude, B, is calculated using the same form factors, and it is also markedly affected. However, when the direct and exchange amplitudes are added coherently in the natural-parity model t, the result is virtually identical to our previous model t. Differential cross sections differ by less than 5% in magnitude and imperceptibly in shape. The shapes of spectra resulting from the natural-parity version of model s are also similar to those of model s, although the depleted region near $(\cos\theta_t, \phi_t) = (0.5, \pi)$ has been partially filled in and the total cross section is five times greater. Model s is considerably more sensitive than is model t to changes in the spin-parity content of the propagator.

---

*Work performed under the auspices of the United States Energy Research and Development Administration.

[1]Rochester-Fermilab-SLAC-Northwestern Collaboration, J. Biel, E. J. Bleser, D. Duke, T. Ferbel, D. Freytag, B. Gobbi, L. Kenah, J. Rosen, R. Ruchti, P. Slattery, and D. Underwood, Phys. Rev. Lett. 36, 504 (1976); 36, 507 (1976); Phys. Lett. B65, 291 (1976); and private communications. Data from this collaboration are referred to as the "Fermilab data" in the text. Neutron diffraction dissociation has also been studied at the CERN ISR by the CERN-Pavia-Zurich Collaboration, G. C. Mantovani *et al.*, Phys. Lett. B64, 471 (1976); B65, 401 (1976).

[2]CERN-Hamburg-Orsay-Vienna ISR Collaboration, H. de Kerret, E. Nagy, M. Regler, W. Schmidt-Parzefall, K. R. Schubert, K. Winter, A. Brandt, H. Dibon, G. Flügge, F. Niebergall, P. E. Schumacher, J. J. Aubert, C. Broll, G. Coignet, J. Favier, L. Massonnet, M. Vivargent, W. Bartl, H. Eichinger, Ch. Gottfried, and G. Neuhofer, Phys. Lett. B63, 477 (1976); B63, 483 (1976).

[3]ITEP-Moscow-Karlsruhe-CERN Collaboration, A. Babaev *et al.*, CERN report, 1976 (unpublished).

[4]S. D. Drell and K. Hiida, Phys. Rev. Lett. 7, 199 (1961); R. T. Deck, *ibid.* 13, 169 (1964).

[5]E. L. Berger, Phys. Rev. 166, 1525 (1968); 179, 1567 (1969); G. Ascoli *et al.*, Phys. Rev. D 9, 1963 (1974).

[6]E. L. Berger, Argonne Report No. ANL-HEP-PR-7506, 1975 (unpublished); E. Berger, in *Proceedings of the Daresbury Conference on Analysis of Three-Particle Decays and Meson Resonance Production, 1975*, edited by J. B. Dainton and A. J. G. Hey (Daresbury Nuclear Physics Laboratory, Daresbury, Warrington, Lancashire, England, 1975).

[7]E. L. Berger, Phys. Rev. D 11, 3214 (1975).

[8]P. Bosetti *et al.*, Nucl. Phys. B103, 189 (1976).

[9]M. Ross and Y. Y. Yam, Phys. Rev. D 1, 2494 (1970); W. Ochs *et al.*, Nucl. Phys. B102, 405 (1976); H. R. Gerhold and W. Majerotto, Nuovo Cimento 36A, 271 (1976).

[10]A. Minaka, H. Sumiyoshi, and M. Uehara, Prog. Theor. Phys. 57, 169 (1977).

[11]E. L. Berger and G. C. Fox, Nucl. Phys. B26, 1 (1971).

[12]E. L. Berger and P. Pirilä, Phys. Lett. 59B, 361 (1975); V. A. Tsarev, Phys. Rev. D 11, 1864 (1975); E. L. Berger and P. Pirilä, *ibid.* 11, 3448 (1975).

[13]E. L. Berger and P. Pirilä (unpublished).

[14]J. L. Basdevant and E. L. Berger, Phys. Rev. Lett. 37, 977 (1976).

[15]M. J. Levine, AEC Report No. CAR-882-25, 1971 (unpublished).

[16]Ross and Yam, Ref. 9; G. C. Fox, in *Experimental Meson Spectroscopy—1972*, proceedings of the Third International Conference, Philadelphia, edited by K.-W. Lai and A. H. Rosenfeld (A.I.P., New York, 1972).

[17]R. T. Cutler and H. W. Wyld, Phys. Rev. D 12, 1952 (1975).

[18]Because we have included baryon-exchange terms, our present models evade earlier criticisms of the Deck-model interpretation of mass-slope correlations in Ref. 19. In a recent article, Saclay Report No. DPh-T/76/75, submitted to the Tbilisi Conference, 1976, F. Hayot, A. Morel, A. Santoro, and M. Souza speculate that the structure in $d\sigma/dt_1$ near $t_1 = -0.2$ GeV^2 arises from the cancellation between the direct and baryon-exchange graphs, discussed in Sec. V, Eq. (5.6). E.L.B. is grateful to Dr. C. Meyers, Bordeaux, for bringing this speculation to his attention and for his demonstration that it is quantitatively invalid for $\cos\theta_t \simeq 0$. Nevertheless, the cancellation is

instrumental in increasing b and thus provides the strong mass-slope correlation in our model s. The model described in the Saclay report is asymptotically equivalent to our model s without form factors.

[19]H. I. Miettinen and P. Pirilä, Phys. Lett. 40B, 127 (1972).

[20]The issue of s-channel vs t-channel helicity conservation is reviewed in D.W.G.S. Leith, in Proceedings of the Summer Institute on Particle Physics, SLAC Report No. 179, Vol. 1, 1974 (unpublished); see also E. L. Berger and J. T. Donohue, Phys. Rev. D 15, 790 (1977).

[21]K. N. Watson, Phys. Rev. 88, 1163 (1952).